Nucleic Acids Research, 2025, **53**, gkaf104
https://doi.org/10.1093/nar/gkaf104
NAR Breakthrough Article

Disassembly of unstable RNA structures by an *E. coli* DEAD-box chaperone accelerates ribosome assembly

Yunsheng Sun and Sarah A. Woodson *

T.C. Jenkins Department of Biophysics, Johns Hopkins University, 3400 N. Charles St., Baltimore, MD 21218, United States

*To whom correspondence should be addressed. Email: swoodson@jhu.edu

Abstract

Ribosome synthesis in bacteria is coupled with transcription of the pre-ribosomal RNA (pre-rRNA), which must fold and assemble with 20 or more ribosomal proteins. *In vitro*, the *Escherichia coli* pre-16S rRNA misfolds during transcription, delaying stable binding of ribosomal protein uS4 that nucleates assembly of the 16S 5′ domain. Using single-molecule fluorescence microscopy, we show that the DEAD-box protein CsdA (DeaD) strongly accelerates uS4 binding by facilitating proper folding of the nascent rRNA. Unstable RNA structures are unfolded by CsdA, whereas stable RNA structures resist unwinding. We show that CsdA unfolding becomes less frequent as more ribosomal proteins add to the complex. The results demonstrate that disassembly of unstable, nascent RNA–protein complexes by chaperones fuels the search for native structure. We propose that general chaperones create a gradient of disassembly that steepens the hierarchy of proper protein addition until late assembly intermediates escape unwinding and commit to 30S maturation.

Graphical abstract

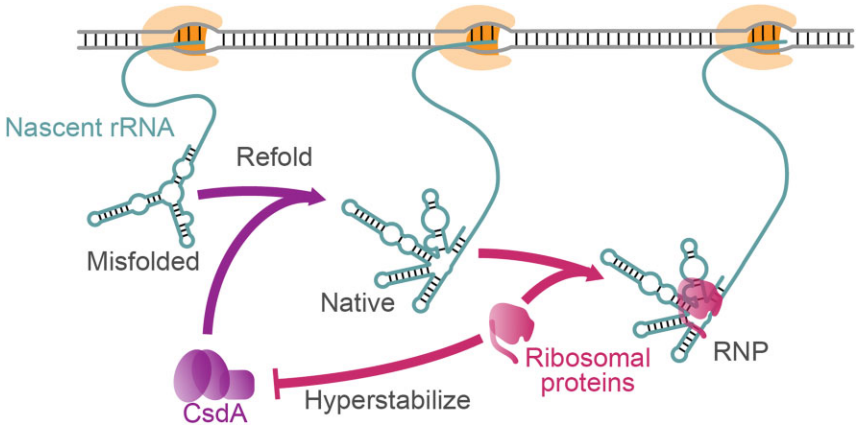

Introduction

Self-assembly of the *Escherichia coli* 30S ribosomal small subunit involves proper folding of the 16S ribosomal RNA (rRNA) and the binding of 20 unique ribosomal proteins. In cells, ribosome assembly is coupled with rRNA transcription [1] and takes ∼2 min [2]. This process can be recapitulated *in vitro* by hierarchical addition of 30S proteins to the native 16S rRNA [3, 4]. Although native ribosomal protein–RNA interactions are stable, recent experiments showed that protein binding during *in vitro* transcription is short-lived and nonproductive, until the RNA has an opportunity to refold [5, 6]. These observations indicated that the pre-rRNA does not inherently fold properly as it is transcribed, but instead becomes temporarily trapped in misfolded conformations that are incompetent to assemble with ribosomal proteins. These observations suggested that efficient cotranscriptional assembly in cells requires chaperones that prevent or correct rRNA misfolding.

Here, we show that ATP-dependent unwinding of newly transcribed rRNA by a DEAD-box RNA chaperone facilitates stable recruitment of ribosomal protein uS4 (S4 hereafter) during early stages of 30S ribosome assembly. Many RNAs are prone to misfolding during transcription because nearby complementary segments in the elongating transcript quickly base pair with each other, preventing essential long-range helices from forming [7]. This competition between local and long-range interactions can delay formation of the correct structure, requiring chaperones to smooth out kinetic

Received: October 10, 2024. **Revised:** January 27, 2025. **Editorial Decision:** January 29, 2025. **Accepted:** February 5, 2025

folding traps [8, 9]. DEAD-box proteins are capable of refolding large, structured RNAs such as group I and group II ribozymes by repeated cycles of ATP-dependent RNA unfolding [10–14]. They are typically nonprocessive unwindases [15] that load onto RNA duplexes internally [16], enabling them to locally remodel large transcripts [17]. RNA binding to the DEAD-box protein drives strand separation, whereas ATP hydrolysis is required for enzyme turnover [18].

DEAD-box chaperones are proposed to act by an iterative annealing mechanism [19, 20], in which each round of ATP-dependent unfolding of the RNA by the chaperone is followed by chaperone-independent refolding. This process is inherently nonselective, because chaperones can unfold native as well as misfolded RNAs, and the RNAs may refold correctly or incorrectly. Theoretical models show, however, that native RNA accumulates over repeated chaperone cycles if misfolded molecules are unfolded more rapidly by the chaperone, or if the native molecules are diverted by downstream reactions [20, 21]. It is not known whether this general chaperone activity facilitates cotranscriptional assembly of ribosomes.

DEAD-box proteins participate extensively in ribosome biogenesis with diverse functions in rRNA processing, ribonucleoprotein (RNP) remodeling, and small nucleolar RNP removal [22–24]. In *E. coli*, four of the five known DEAD-box proteins (DbpA, SrmB, CsdA, RhlE) act in ribosome biogenesis [25]. Among these, CsdA (also named DeaD) is a major cold shock protein that is reported to act widely in gene expression with little known RNA sequence specificity [26, 27]. Deletion of CsdA causes a cold-sensitive phenotype and accumulation of immature 50S subunits [28, 29]. CsdA overexpression was also reported to suppress temperature-sensitive mutations in ribosomal protein uS2, possibly by rescuing suboptimal 30S assembly [30].

To determine whether CsdA can rescue rRNA misfolding during transcription, we used single-molecule fluorescence to monitor rRNA transcription and protein S4 binding at the same time. The results showed that CsdA increases the likelihood of stable S4 binding by temporarily unfolding the nascent rRNA, providing it another chance to fold correctly. When the rRNA structure is unstable, it is rapidly unfolded by CsdA and S4 dissociates. Conversely, when free protein S4 is available, S4 recaptures the rRNA from CsdA. This competition between disassembly and reassembly may serve as a natural checkpoint to prevent fruitless cycles of chaperone unfolding while permitting native-like complexes to form mature 30S ribosomes.

Materials and methods

Reagents

Standard reagents for molecular biology and protein purification are provided in the Supplementary Methods. Reagents used for single-molecule fluorescence microscopy were dichlorodimethylsilane (Sigma, Cat #440272), Tween 20 (Fisher Bioreagents, Cat #BP337), biotin-conjugated bovine serum albumin (Sigma, Cat #A8549), neutravidin (Thermo Fisher, Cat #31000), Trolox (Acros Organics, Cat #AC218940010), glucose oxidase (Sigma, Cat #G2133), glucose (Sigma, Cat #G8270), and RNasin plus (Promega, Cat #N2611). Commercial kits included NucleoSpin Gel and PCR Clean-up (Takara, Cat #740609), Q5 Site-Directed Mutagenesis Kit (NEB, Cat #E0554S), NEBuilder HiFi Assembly Master Mix (NEB, Cat #E2621S), and RNeasy Mini Kit (QIAGEN). Custom oligonucleotides and primers are listed in Supplementary Table S1.

Biological resources

CsdA coding sequence, protein S4 sequence, and 16S rRNA sequence were derived from the K-12 strain of *E. coli*. Proteins were overexpressed from plasmids and purified from *E. coli* BL21(DE3) cells as described below. Ribosomes were purified from *E. coli* MRE600. Molecular cloning was performed in *E. coli* DH5α. Scarless, in-frame deletion of *rbfA* in parental strain BW25113 was generated in this study following the no-SCAR protocol [31, 32]. The entire *rbfA* open reading frame was deleted except for the start codon and the last six amino acids. The desired junction was confirmed by colony polymerase chain reaction (PCR) and Sanger sequencing.

Protein expression, purification, and labeling

Escherichia coli ribosomal protein S4 (C32S, S189C) was purified and labeled with maleimide-Cy3 dye (GE Healthcare) as previously described [33]. T7 RNA polymerase [34] and other ribosomal proteins [35] were overexpressed and purified as previously described. Full-length *E. coli* CsdA with an N-terminal His-tag followed by a TEV protease site was overexpressed from pET28 CsdA_FL [36], as described in the Supplementary Text.

In vitro transcription templates

DNA templates for *in vitro* transcription of the *E. coli* 16S five-way helix junction (5WJ) [37] and 16S 5′ domain (nucleotides 26–556) [38] were adapted for this study (Supplementary Table S2). A T7 promoter and C-less cassette were added to the 5′ end of each template, and an anti-SA5 sequence and T7 terminator were appended to the 3′ end during PCR amplification (Q5 DNA polymerase; NEB) of the desired rRNA sequence [6]. Transcription restarts at 16S C34. A Cy3 fluorophore was added to the downstream end of the template using reverse primer pTerm29_aadU25 containing an aminoalkyl-modified thymine (see Supplementary Table S1). To attach the fluorophore to the primer, 5 nmol primer DNA was dissolved in 66 µl of 100 mM $NaHCO_3$ (pH 8.5) and then combined with Cy3-NHS mono-reactive dye (GE Healthcare) dissolved in 33 µl dimethyl sulfoxide. The reaction was incubated at room temperature overnight, and then cleaned up using a TE10 spin column (Takara) and ethanol precipitation.

Single-molecule fluorescence microscopy

Single-molecule fluorescence microscopy experiments were performed using a home-built total internal reflection fluorescence (TIRF) microscope with an EMCCD camera [39]. Cy3 and Cy5 fluorophores were excited using 532 and 640 nm lasers, respectively. Flow channels were prepared on passivated quartz microscope slides coated with Tween 20 and neutravidin [40].

Nascent rRNA

smCoCoA (single-molecule assay for cotranscriptional assembly) experiments were performed as previously described [6] with some modifications. Transcription elongation complexes (TECs) were assembled in 10 µl using 80 nM Cy3-DNA tem-

plate, 40 mM Tris–HCl (pH 7.5), 20 mM $MgCl_2$, 20 nM T7 RNA polymerase, 200 μM GTP, 200 μM ATP, 50 μM UTP, and 30 nM biotinylated T3-Cy5-biotin DNA complementary to the C-less cassette. The mixture was incubated at room temperature for 20 min, then diluted 50- to 100-fold with 40 mM Tris–HCl (pH 7.5) and 20 mM $MgCl_2$ (100 μl total), and injected into the flow channel for immobilization. The immobilized fluorescent complexes were well separated in the field of view (<500 fluorescent spots per 256 × 512 pixels; Supplementary Fig. S1A). After immobilization, free DNA template was removed with 100 μl imaging buffer [40 mM Tris–HCl, pH 7.5, 4–40 mM $MgCl_2$, 150 mM KCl, 1% (w/v) glucose, 165 U/ml glucose oxidase, 4 mM Trolox].

Movies were recorded with 9 frames of 640 nm excitation (100 ms per frame) to check for the presence of an active Cy5 fluorophore, 3000 frames (5 min) of 532 nm (Cy3) excitation, followed by 9 frames of 640 nm excitation to monitor Cy5 photobleaching. During Cy3 excitation, transcription was restarted with 100 μl restart buffer [40 mM Tris–HCl, pH 7.5, 4–40 mM $MgCl_2$, 150 mM KCl, 1 mM ATP, 1 mM CTP, 1 mM UTP, 1 mM GTP, 1% (w/v) glucose, 165 U/ml glucose oxidase, 4 mM Trolox] containing 2.5–5 nM Cy3-S4 and 0–400 nM CsdA.

Refolded rRNA

The rRNA was transcribed *in vitro*, purified by polyacrylamide gel electrophoresis (PAGE), and renatured with the desired antisense oligonucleotides as follows. To measure S4 binding, 10 nM rRNA was combined with 10 nM T3-Cy5 and 10 nM biotinylated SA5-biotin oligonucleotides that are complementary to the C-less and SA5 sequence tags at the 5′ and 3′ ends of the rRNA, respectively. To measure CsdA unwinding, 10 nM rRNA was combined with 10 nM T3-Cy5-biotin and 10 nM SA5-Cy3 oligonucleotides. The RNA was renatured with the antisense oligonucleotides by heating to 75°C for 5 min and cooling to 37°C over 30 min in 40 mM Tris (pH 7.5) and 150 mM KCl. The desired concentration of $MgCl_2$ was added, and the reaction incubated for a further 5 min at 37°C. Ribosomal protein–rRNA complexes were prepared by adding 20 nM S4, 240 nM S16, 80 nM S17, and 80 nM S20 proteins to the renatured RNA for another 5 min at 37°C. The mixture was diluted ∼20-fold and introduced into the slide chamber for imaging as described earlier. Movies were recorded with the same excitation scheme as nascent rRNA. The experiments were performed in restart buffer with CsdA.

RNase H cleavage

Mature 30S ribosomes and native 16S rRNA were purified from MRE600 [41]. 30S subunits or 16S rRNA was diluted in 40 mM Tris (pH 7.5), 150 mM KCl, 4 mM $MgCl_2$, 1 mM NTP, and 3 mM dithiothreitol (DTT) to 100 nM and combined with 33 μM complementary DNA oligomer (20 μl total volume). To start the reaction, CsdA was added to 200 nM. After 5 min at room temperature, $MgCl_2$ was added to 20 mM to stop CsdA unwinding and DNA hybridization. RNase H was immediately added to 0.1 U/μl. After 5 min, reactions were quenched with 14 μl of 62% formamide, 2% sodium dodecyl sulfate, and 90 mM ethylenediaminetetraacetic acid (EDTA). Products were treated with 2 mg/ml proteinase K for 5 min, then diluted 10 times in formamide, resolved by 6% PAGE (tris-borate EDTA buffer (TBE) with 8 M urea), and stained with SYBR Gold (Invitrogen).

Plate assay for CsdA overexpression

Plasmids that express CsdA (pMAL-p5X-CsdA) or CsdA-DQAD (pMAL-p5X-CsdA-DQAD) were generated by replacing the MBP coding sequence with the desired coding sequence in pMAL-p5X using HiFi Assembly (NEB). The plasmids were used to transform wild-type (WT; BW25113) and Δ*rbfA* strains. For each strain, three transformed colonies were selected from LB agar with 100 mg/l ampicillin and used to inoculate overnight cultures in LB/ampicillin. Five microliters of serial dilutions (10^0, 10^{-1}, 10^{-2}, 10^{-3}, 10^{-4}) were spotted on LB agar + 100 mg/l ampicillin plates with (0.25 mM) or without isopropyl β-D-1-thiogalactopyranoside (IPTG), and incubated at 37°C for 24 h.

Statistical analyses

Single-molecule image analysis

Recorded videos were analyzed using Imscroll [42]. For co-transcriptional binding experiments, immobilized TECs with active Cy3 and Cy5 fluorophores were picked using an automatic spot-detection algorithm in Imscroll. Any areas of interest with more than one molecule were excluded from further analysis (<5%). The Cy3 and Cy5 intensities were calculated for each frame with rolling ball background subtraction [42]. A protein-induced fluorescence enhancement (PIFE) signal was taken to signify successful transcription of the DNA template; TECs without a PIFE signal were not analyzed further. For experiments with refolded rRNA, a few frames of red excitation at the beginning of the movie were used to pick immobilized RNA molecules. For unfolding/refolding experiments, all immobilized RNA molecules with active Cy3 and Cy5 fluorophores were analyzed. Nearly all molecules exhibited high Förster resonance energy transfer (FRET) efficiency at the start of the experiments (before the addition of CsdA).

Detection of S4 binding events

Intervals of S4 binding were defined by an increase in the sum of Cy3 and Cy5 intensities [43]. To determine the FRET efficiency, leakage from the donor to acceptor channel was estimated using frames with nonspecific Cy3-S4 binding, which does not produce FRET. After subtracting the background and the donor leakage, the FRET efficiency was calculated by $E_{FRET} = I_{acceptor}/(\gamma \times I_{donor} + I_{acceptor})$, in which $\gamma = \Delta I_{acceptor}/\Delta I_{donor}$ $(1.0 < \gamma < 1.5)$ is the correction factor that depends on the accuracy of mapping and the difference in the quantum yield of the donor and acceptor [39]. The correction factor was determined for each experiment.

Binding lifetimes

The duration of S4 binding events was fitted by a triple exponential distribution with the maximum likelihood method [42, 43] to yield characteristic binding lifetimes (τ) and amplitudes (a) or the probability of a binding event falling into binding mode with lifetime τ. Errors were estimated by bootstrap resampling [6]. The threshold for stable binding was chosen to be 20 s, which is 10 times longer than the transient binding time constant (2 s), yet much shorter than characteristic stable binding. Cy3 photobleaching was infrequent (<10% during 300 s imaging) and did not appreciably affect the estimate of S4 occupancy.

FRET efficiency

The FRET efficiency of stable binding events ($t > 20$ s) was fitted by a double Gaussian distribution to obtain the mean FRET efficiencies, E_{FRET}, of the high-FRET and low-FRET states. Specific binding events were defined as having $E_{FRET} > 0.05$. This threshold is lower than E_{FRET} of the low-FRET state, yet sufficient to rule out nonspecific binding.

S4 occupancy

The S4 occupancy was defined as the proportion of time that immobilized rRNAs were stably ($t > 20$ s) and specifically ($E_{FRET} > 0.05$) bound by S4, averaged across all molecules in a given experiment (~100 molecules per replicate). The occupancy was calculated separately for each replicate of the experiment. The numbers of replicates and molecules used for each experiment are listed in Supplementary Table S3. One-way analysis of variance (ANOVA) was performed on the mean occupancy values determined from each replicate to check the significance of our hypothesis.

Other analysis

The initial binding time of S4 was fitted using a single exponential function

$$f_1(t) = a_1(1 - e^{-k_1 t})$$

or a double exponential function

$$f_2(t) = a_1(1 - e^{-k_1 t}) + a_2(1 - e^{-k_2 t})$$

using least-squares fitting. The 95% confidence bounds were calculated using the Jacobian of the fitted value with respect to the coefficients and the mean squared error. The mean FRET efficiency of native rRNA versus time was fitted using exponential functions $a_0 - f_1(t)$ or $a_0 - f_2(t)$, where a_0 is the FRET value before CsdA addition. The fraction of S4 dislodged by CsdA was fitted using $f(t) = e^{-k_1 t}$.

Novel programs, software, and algorithms

Custom scripts for data analysis may be obtained from Johns Hopkins Research Data Repository at http://doi.org/10.7281/T1/Z73MRN.

Results

smFRET detects site-specific S4 binding to nascent rRNA

Protein S4 nucleates assembly of the 16S 5′ and central domains [44] by recognizing the folded structure of a 5WJ near the 5′ end of 16S rRNA [37, 45–48] (Fig. 1A). After S4 binds, the S4–16S rRNA encounter complexes go through a conformational change that produces a stable native complex [38, 49, 50]. Both initial binding of the 5WJ and subsequent remodeling of the S4–16S complex require formation of the native rRNA structure [47, 51, 52]. We previously observed that ribosomal protein S4 frequently binds the pre-16S rRNA during transcription *in vitro*, but most binding events last only a few seconds [6]. Short-lived binding may represent either unproductive encounters with S4's proper binding site or nonspecific binding to other sites in the rRNA. To distinguish these possibilities, we combined an smCoCoA with single-molecule FRET (smFRET) detection of specific S4 binding to the 16S 5WJ [6, 38]. For these experiments, we transcribed either an rRNA fragment containing only the minimal 5WJ S4 binding site or the 16S 5′ domain that forms the body of the 30S ribosome (Fig. 1A and B).

To visualize S4 binding immediately after transcription, we assembled stalled T7 TECs in the absence of CTP, using a C-less sequence at the start of the template (Fig. 1C). Stalled TECs were immobilized on the surface of a passivated quartz slide via a biotinylated DNA oligomer hybridized to the 5′ end of the nascent RNA (Fig. 1D) and imaged by TIRF microscopy. The DNA template was labeled with Cy3 fluorophore, and the tether DNA was labeled with Cy5 fluorophore, allowing genuine TECs to be identified by colocalization of Cy3 and Cy5 signals (Supplementary Fig. S1). Transcription was restarted with the addition of all four NTPs (Fig. 1D), and its completion was denoted by PIFE [53] when T7 RNA polymerase moves over the Cy3 fluorophore attached to the downstream end of the DNA template (Fig. 1E). The large increase in Cy3 intensity due to PIFE and subsequent release of the Cy3-DNA template (Supplementary Fig. S1) were only observed after the addition of NTPs and were used to identify restarted TECs.

To monitor S4 binding, 5 nM Cy3-labeled S4 was added together with the NTPs. Specific S4 binding to the 5WJ was detected by FRET (Fig. 1E and F) between the Cy3 donor fluorophore attached to S4 and a Cy5 acceptor fluorophore attached to the DNA hybridized with the 5′ end of the RNA (Fig. 1D). When S4 binds nonspecific sites, the two fluorophores colocalize without FRET [6]. As expected, we observed both transient and long-lived S4 colocalization with both RNAs, reflecting a mixture of unstable and stable S4 complexes (Fig. 1D and E, and Supplementary Fig. S2). Most binding events occurred after these short DNA templates were completely transcribed (~10 s; Fig. 1E) because the S4 binding site lies near the 3′ end of the transcript. However, S4 binding during the 5-min video largely reflects rRNA structures formed during transcription because spontaneous rRNA refolding at 25°C is very slow (>10 min) [54].

As ribosomal proteins only form stable complexes with properly folded rRNA, the frequency of stable binding reflects the native rRNA population [5, 6]. To assess the likelihood of stable binding, the distribution of all S4 dwell times was fitted by three exponential decay functions, yielding average dwell times for transient binding ($\tau_1 = 0.24 \pm 0.01$ s), short-lived binding ($\tau_2 = 1.8 \pm 0.3$ s), and stable binding ($\tau_3 > 300$ s) (Fig. 1G and Supplementary Table S4). These binding modes were also observed by S4 colocalization during pre-16S transcription [6]. Previous experiments showed that S4–rRNA complexes fluctuate between a native high-FRET conformation in which 16S helix 3 is docked against S4 (Fig. 1D) and an intermediate low-FRET conformation in which helix 3 flips away from S4 [38]. In our current experiments, nearly all stable S4 binding events ($t \geq 20$ s) with the nascent 5WJ (90%) or 5′ domain RNA (80%) sampled the high-FRET state at least once (Fig. 1H and Supplementary Fig. S2), indicating that these stable events corresponded to specific recognition of the native 5WJ. We set $E_{FRET} > 0.05$ as the criterion for site-specific binding, which was sufficient to exclude nonspecific binding to other sites in the rRNA. The similarity between these results and previous results showed that our smFRET assay faithfully reports specific S4 binding to nascent transcripts.

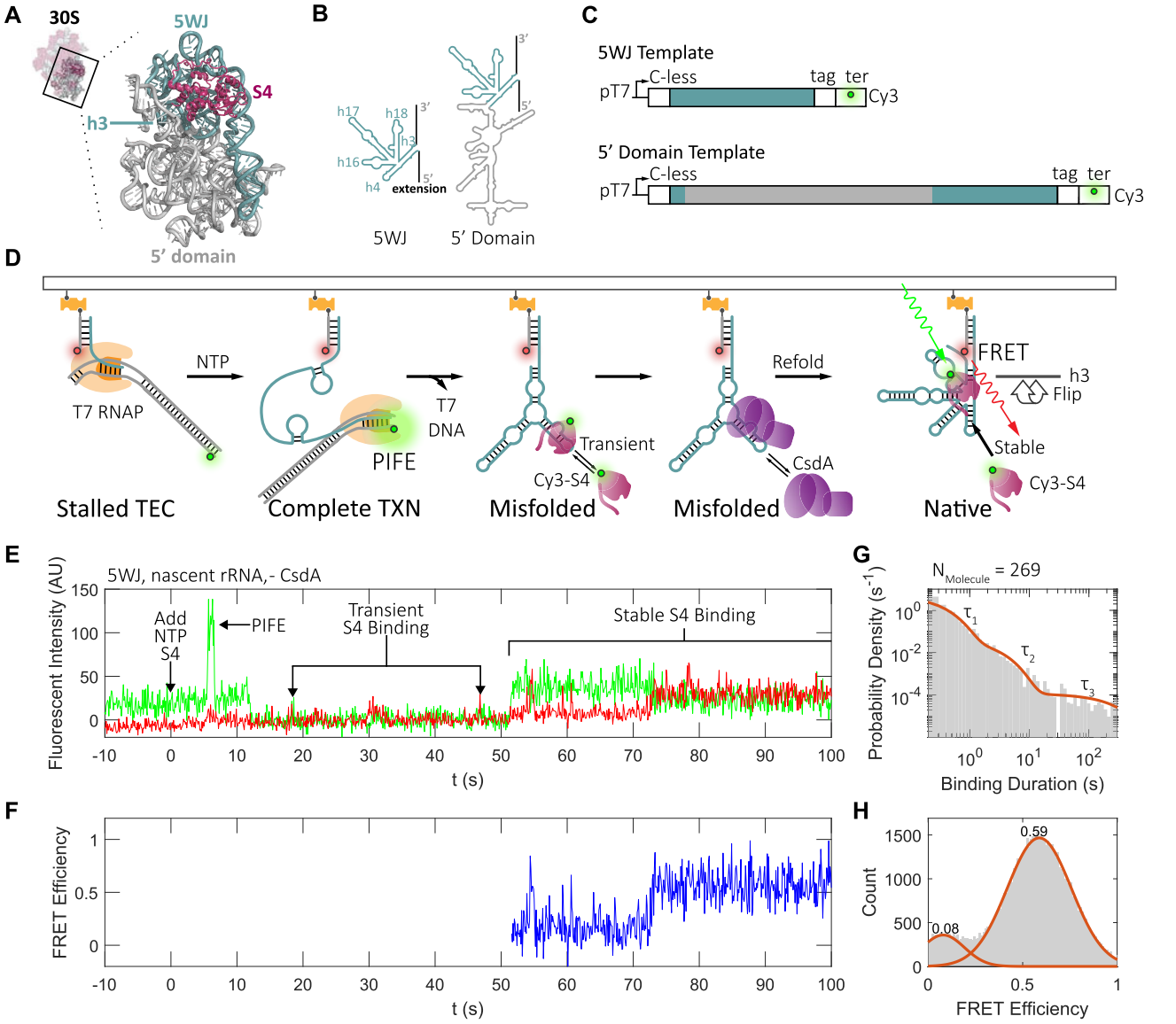

Figure 1. Single-molecule fluorescence monitors binding of *E. coli* S4 with nascent rRNA. (**A**) Protein S4 binds the 16S 5WJ (teal) at an early step of 30S ribosome assembly. Ribbon from PDB 4V9D [80]. (**B**) Secondary structures of *E. coli* 16S 5WJ and 5′ domain RNAs used in this study. (**C**) DNA templates for cotranscriptional assembly. C-less, C-less cassette for stalling transcription; tag, sequence tag (see Supplementary Table S2); ter, T7 terminator. (**D**) smFRET monitors specific binding of S4 to nascent rRNA. Stalled TECs were assembled, immobilized, and restarted as described in the "Materials and methods" section. PIFE reports complete transcription of each template. Nonspecific Cy3-S4 binding results in Cy3 and Cy5 colocalization without FRET; specific binding to the 5WJ results in FRET. Example single-molecule trace illustrating nonspecific and stable specific binding with nascent 5WJ rRNA; 1 mM each NTP and 5 nM Cy3-S4 were added at time 0: (**E**) fluorophore intensities after background subtraction; (**F**) FRET efficiency of stable S4 binding. See Supplementary Fig. S2 for additional examples. (**G**) Probability density of S4 binding duration for nascent 5WJ rRNA (gray bars) fitted by three exponential decays (orange curve) using maximum likelihood [43]. Lifetimes were $\tau_1 = 0.24 \pm 0.01$ s, $\tau_2 = 1.8 \pm 0.3$ s, $\tau_3 \geq 1.0 \pm 1.7 \times 10^3$ s (see Supplementary Table S4). Errors are from bootstrap resampling (see the "Materials and methods" section). The time constant of the stable binding mode is a lower bound limited by the total video recording time (300 s). (**H**) FRET efficiency of stable S4 binding events on nascent 5WJ rRNA reveals the same native (h3 docked; $E_{FRET} = 0.59$) and intermediate (h3 undocked; $E_{FRET} = 0.08$) conformations observed on refolded RNA [38]. Gray bars, data; orange line, fit. See Supplementary Fig. S2 for further data.

CsdA helicase promotes specific S4 recruitment

If the likelihood of stable S4 recruitment is low because the rRNA misfolds during transcription, we hypothesized that a DEAD-box chaperone such as CsdA could rescue assembly by refolding the rRNA through a general iterative annealing mechanism. We confirmed that CsdA rapidly unwinds a 21-bp RNA duplex with a single mismatch under our cotranscriptional ribosome assembly conditions, but slowly unwinds a perfectly matched duplex (Supplementary Fig. S3). This substrate preference suggested that CsdA can act on the varied RNA secondary structures formed during transcription as long as they are not too stable.

In the absence of a chaperone, long-lived S4 binding events were rarely observed after transcription (Fig. 2A). The probability that a 5WJ transcript was stably bound by S4 ($t \geq 20$ s) at any point during the 5-min video was only 20% (Supplementary Fig. S4B). For the nascent 5′ domain RNA, this probability dropped to 10% (Supplementary Fig. S4C), although the longer transcript experienced a greater number

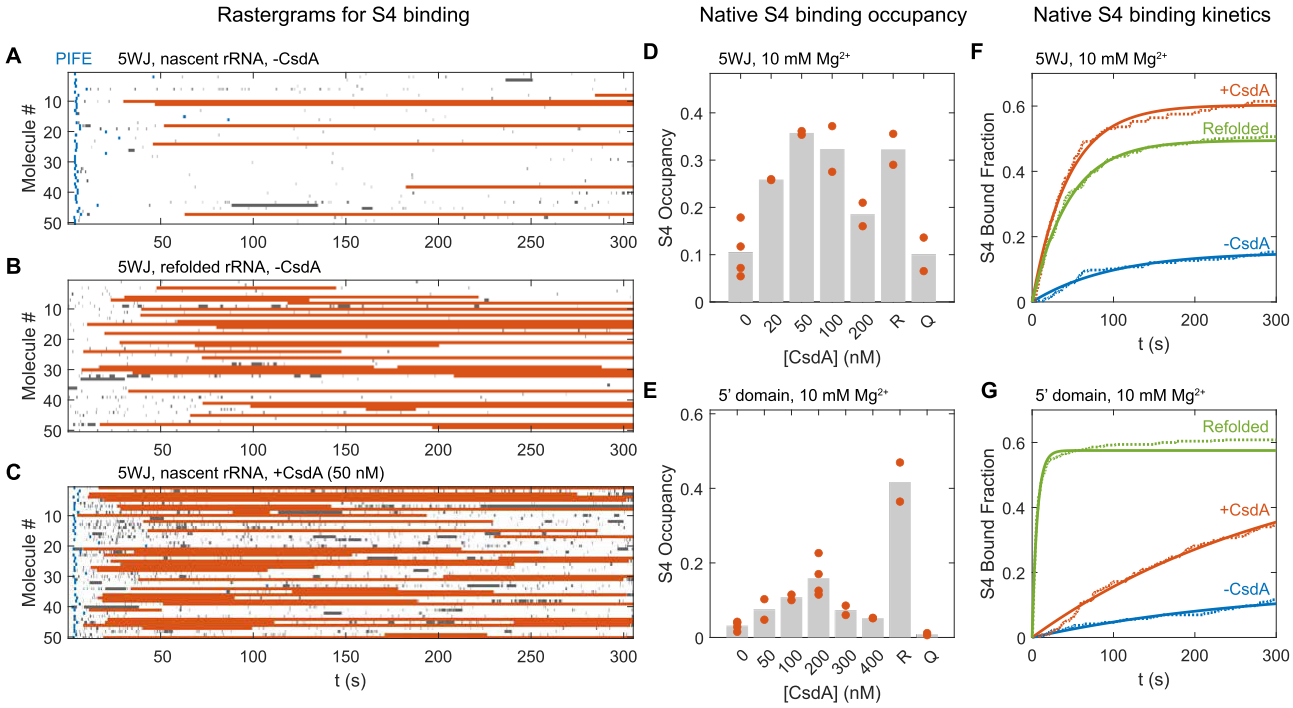

Figure 2. CsdA DEAD-box ATPase promotes S4 recruitment to nascent rRNA. (**A**–**C**) S4 binding kinetics. Each row of the rastergram represents a single transcript selected at random from restarted TECs (A,C) or a refolded RNA (B). Blue dots, end of transcription (PIFE); orange bars, site-specific S4 binding; gray bars, nonspecific binding as in Fig. 1E. Fewer than 10% of Cy3 fluorophores were photobleached in 300 s. (A) Nascent 5WJ from the time of NTP addition. (B) Refolded 5WJ from the time of S4 addition. (C) Nascent 5WJ with 50 nM CsdA. See Supplementary Fig. S4 for further data on the 5′ domain. Occupancy of S4 defined as the fraction of time spent in specific complexes (t_{dwell} > 20 s, E_{FRET} > 0.05), averaged over the population of active TECs: (**D**) 5WJ and (**E**) 5′ domain. Orange symbols, averaged over one trial (~100 molecules); gray bars, average of independent trials. 5 nM Cy3-S4 in 40 mM Tris–HCl (pH 7.5), 10 mM $MgCl_2$, 150 mM KCl plus 0–200 nM CsdA. R, refolded rRNA; Q, 50 nM (D) or 200 nM (E) CsdA-DQAD. See Supplementary Fig. S4 for further data, Supplementary Fig. S6 for comparison with iterative annealing models, and Supplementary Table S5 for results of one-way ANOVA. (**F**, **G**) S4 recruitment kinetics. Cumulative fraction of complexed 5WJ rRNAs (F) or 5′ domain rRNAs (G) that have formed a stable specific complex versus the initial time of specific S4 binding. Dashed curve, raw data; solid curve, fit by single exponential rise. Blue, nascent RNA − CsdA; orange, nascent RNA + 50 or 200 nM CsdA; green, refolded RNA. See Supplementary Table S6 for kinetic parameters.

of S4 binding events overall (Supplementary Fig. S4D). When either the 5WJ or 5′ domain RNAs were refolded in 10 mM $MgCl_2$ before adding S4, however, the proportion of stable binding events rose to 60% (Fig. 2B and Supplementary Fig. S4B, C, and E). Nearly all (98%) of the stable complexes were site-specific, as judged by their FRET efficiencies. In addition, renaturation of the RNA reduced the frequency of nonspecific binding (Supplementary Fig. S4F and G). Thus, proper rRNA folding increases stable, specific S4 binding, as expected.

When 50 nM CsdA was added to the transcription reaction, S4 binding to the nascent 5WJ rRNA increased substantially and the pattern of binding resembled reactions with refolded rRNA (Fig. 2C and Supplementary Fig. S4B). CsdA also increased specific binding to the nascent 16S 5′ domain, albeit to a smaller degree (Supplementary Fig. S4C and H). An inactive variant with a mutation in the ATPase site, CsdA-DQAD, had no positive effect on specific S4 binding to the 5WJ (Fig. 2D and Supplementary Fig. S4I) or the 5′ domain RNAs (Fig. 2E and Supplementary Fig. S4J). This result confirmed that the helicase activity of CsdA is required to stimulate stable S4 recruitment to the nascent rRNA.

To determine whether the requirement for CsdA is due to transcription by T7 RNA polymerase in our experiments, we performed additional cotranscriptional assembly reactions using native *E. coli* RNA polymerase (*E. coli* RNAP) under the same conditions. As expected, *E. coli* RNAP took longer to transcribe the 5WJ. However, slower transcription did not increase the proportion of properly folded nascent rRNA, and CsdA was still required to increase the frequency of stable S4 binding (Supplementary Fig. S5).

Optimal chaperone levels depend on RNA length

To evaluate how much CsdA is required to facilitate productive S4 recruitment to the nascent rRNA, we calculated the S4 occupancy as the fraction of time the population of restarted TECs spent in stable, specific S4 complexes. As more CsdA was added, up to 50 nM, the average S4 occupancy increased (Fig. 2D). Above 50 nM, additional CsdA reduced S4 occupancy. The drop in S4 binding at high CsdA was not due to ATP exhaustion, since the theoretical ATP consumption was much lower than the total [55], and CsdA continued to unwind the RNA for >5 min under our reaction conditions. Instead, this negative effect at high CsdA concentrations is likely due to excessive unwinding of the native rRNA, as predicted by the iterative annealing mechanism [20]. A peak in the yield of native RNA with chaperone concentration was also observed for DEAD-box proteins that refold group I and II introns [12, 56]. We found that simulations of iterative annealing recapitulate S4 occupancy of the 5WJ and 5′ domain RNAs, if we assume that more than one CsdA cooperatively unfolds the native RNA (Supplementary Text and Supplementary Fig. S6). At the optimum of 50 nM CsdA, the apparent rate of stable S4 binding to the nascent 5WJ RNA

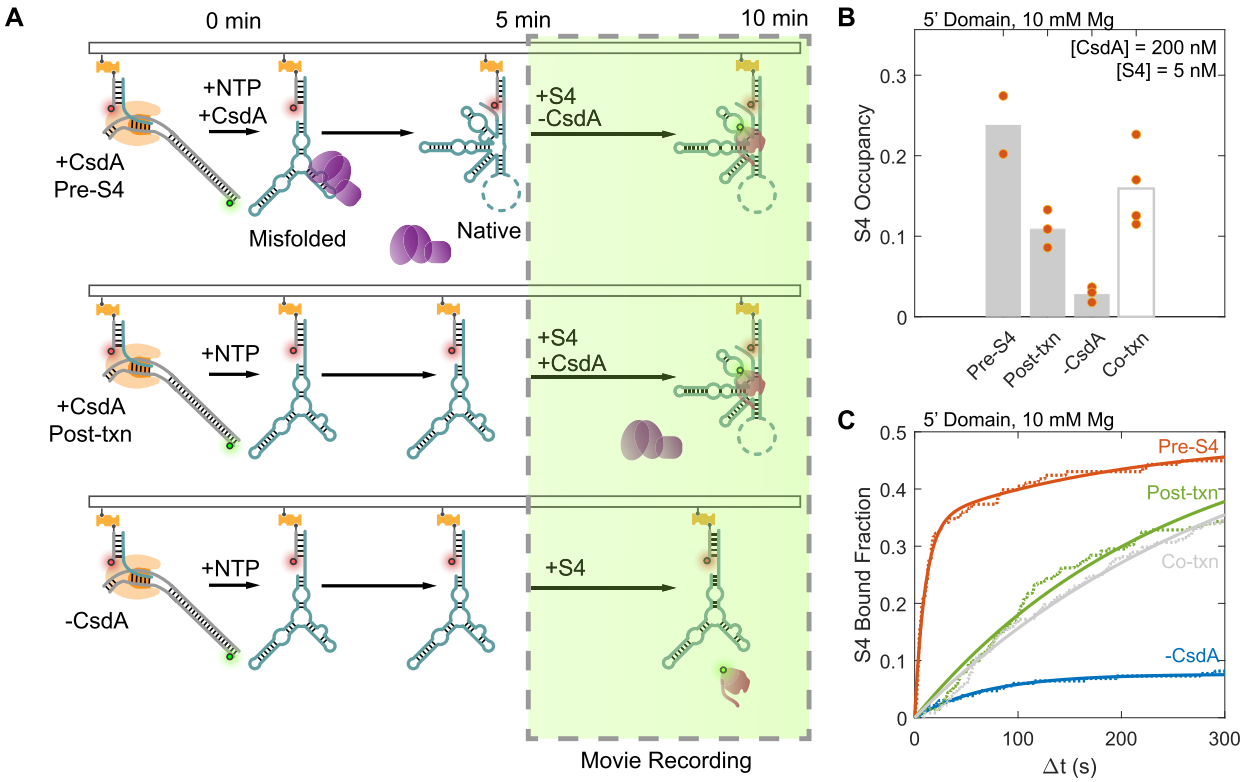

Figure 3. CsdA promotes S4 binding by independently refolding the rRNA. (**A**) Order of CsdA and S4 addition. For all trials, NTPs were added at time 0 to restart transcription and the rRNA was incubated 5 min before the recording was started and 5 nM Cy3-labeled S4 was added. Top: 200 nM CsdA was added during transcription (0 min) and washed away before S4 addition (5 min). Middle: CsdA and S4 were added together (5 min). Bottom: no CsdA control. (**B**) S4 occupancy of nascent 5′ domain in experiments diagrammed in panel (A), compared to co-addition of S4 and CsdA during transcription from Fig. 2E. Symbols, individual replicas; bars, average. See Supplementary Fig. S7 for rastergrams of single TECs and Supplementary Table S5 for statistics. (**C**) S4 recruitment kinetics, from the cumulative fraction of 5′ domain rRNA versus the initial time of stable and specific S4 binding as in Fig. 2F and G. Movie recording started at 5 min. Symbols as in Fig. 2F. Co-txn, data from Fig. 2G. See Supplementary Table S6 for parameters and error analysis.

($0.023\ s^{-1}$; $k_{on} \sim 4 \times 10^6\ M^{-1}\ s^{-1}$) was comparable to the rate of S4 binding to thermally refolded 5WJ RNA (Fig. 2F). Thus, the folding kinetics of the 5WJ no longer limits the rate of assembly in the presence of the chaperone.

CsdA also promoted specific S4 binding to the 5′ domain rRNA (Fig. 2E). However, the optimum quantity of CsdA shifted to 200 nM (Fig. 2E), versus 50 nM for the shorter 5WJ rRNA. Moreover, the maximum S4 occupancy at 200 nM CsdA over the 5-min movie was lower than that of the refolded 5′ domain RNA, corresponding to slower S4 recruitment overall (Fig. 2G). This cannot be due to insufficient chaperone as the CsdA copy number is many times higher than the immobilized RNA even at the lowest concentrations. Instead, CsdA may refold the 5′ domain rRNA less efficiently than the 5WJ because unwinding the larger RNA requires more unfolding cycles, or because the larger RNA is less likely to refold correctly. This length dependence suggests that the chaperone requirement scales with the number of RNA interactions to be refolded.

CsdA can refold the rRNA during or after transcription

We hypothesized that CsdA increases S4 binding by unfolding RNA structures created during transcription, giving the RNA a second chance to refold correctly. However, it is possible that CsdA guides the initial folding of the rRNA during transcription or directly recruits S4 to the rRNA. To evaluate these alternatives, we varied the order in which CsdA and S4 were added to the rRNA (Fig. 3A). First, to test whether CsdA acts on the rRNA or the S4–rRNA complex, the 16S 5′ domain was transcribed with CsdA only (+CsdA, pre-S4). After 5 min, CsdA was washed out of the slide chamber, and Cy3-S4 was added. Sequential addition of CsdA and S4 raised rather than lowered S4 occupancy (Fig. 3B) and accelerated S4 binding (Fig. 3C). This is presumably because CsdA had 5 min to refold the rRNA before S4 was added, increasing the number of transcripts that were competent for assembly. These results showed that CsdA acts on the RNA, not S4.

Next, to test whether CsdA must be present during transcription to have an effect, CsdA and S4 were added together 5 min after transcription was restarted (+CsdA, post-txn). The results were compared to experiments in which CsdA and S4 were added together at the start of transcription (Fig. 2E and G) and to a −CsdA control. CsdA increased S4 occupancy in both experiments (Fig. 3B and Supplementary Fig. S7), indicating that CsdA need not be present during transcription to actively facilitate rRNA refolding.

Chaperone-assisted assembly depends on rRNA stability

Iterative annealing models predict that chaperones will act most efficiently when there is a large free energy gap between the native structure and non-native structures [9, 57]. In the absence of chaperone, occupancy of S4 on the nascent 5WJ

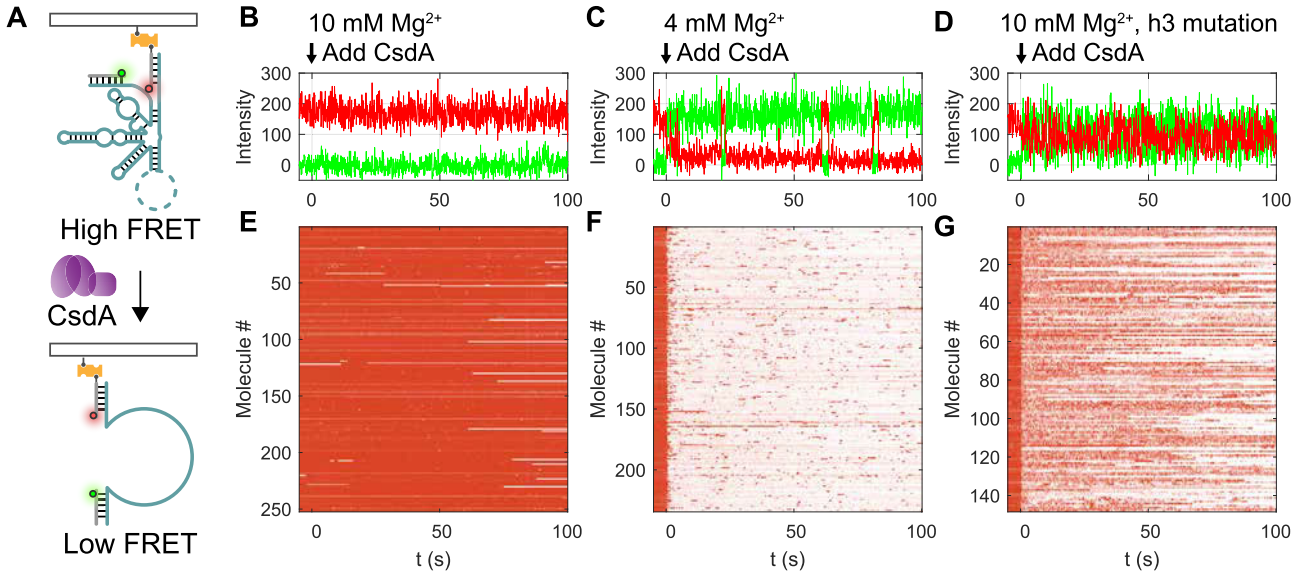

Figure 4. CsdA preferentially unfolds unstable rRNA structures. (**A**) smFRET assay for rRNA unfolding. Renatured rRNA was annealed with fluorescent DNA oligomers (T3-Cy5-biotin and SA5-Cy3) before immobilization and exposure to CsdA. (**B**) Example trace of stably folded 5′ domain rRNA in 10 mM $MgCl_2$ after addition of 200 nM CsdA at time 0. (**C**) Unstable 5′ domain RNA in 4 mM $MgCl_2$, as in panel (B). Once CsdA is added, the RNA spends most of the time in the unfolded, low-FRET state, except for occasional fluctuations to the folded, high-FRET state. (**D**) 5′ domain RNA with mutations that destabilize the helix adjacent to the fluorophores (h3) in 10 mM $MgCl_2$. (**E–G**) Rastergram for CsdA unfolding rRNA as in panels (B)–(D). The FRET values were mapped to a color gradient in which orange represents high FRET efficiency and white represents no FRET.

rRNA was highest at 6–10 mM Mg^{2+} and lower in 20 and 40 mM Mg^{2+} (Supplementary Fig. S8A). This is because very high Mg^{2+} overstabilizes the RNA structure and impedes refolding of nascent transcripts and restructuring of S4–rRNA complexes [38, 48, 58]. To determine how the stability of the folded RNA affects chaperone-assisted assembly, we tested the performance of CsdA at high and low magnesium concentrations. In 10–20 mM Mg^{2+} + NTPs, in which the rRNA structure is moderately stable, 200 nM CsdA increased S4 occupancy of the nascent 16S 5′ domain rRNA (Supplementary Fig. S8B), as expected. At 4 mM Mg^{2+} + NTPs, in which the rRNA structure is barely stable, 200 nM CsdA abolished S4 binding (Supplementary Fig. S8B), presumably because the rRNA is vulnerable to complete unfolding by CsdA. This result was consistent with CsdA's greater unwinding of unstable than stable RNA substrates [59, 60] and a mismatched duplex over a matched duplex (Supplementary Fig. S3). Altogether, these results suggested that chaperone-assisted assembly depends on a balance between CsdA unfolding RNAs that are incompetent to successfully add S4 and the escape of native S4–rRNA complexes from unfolding by CsdA.

CsdA preferentially unfolds unstable rRNA structure

To test whether stable rRNA structure can resist unfolding by CsdA, we used smFRET to directly observe unfolding of renatured 5′ domain rRNA at different magnesium concentrations. To monitor unfolding, the rRNA was thermally renatured and the 5′ and 3′ ends hybridized with Cy5- and Cy3-labeled oligonucleotides (Fig. 4A). Proper folding of the 5′ domain rRNA brings the donor and acceptor fluorophores together, resulting in high FRET. When the rRNA unfolds, the fluorophores are separated, resulting in a loss of FRET.

At 10 mM $MgCl_2$ + NTPs, the renatured rRNA remained folded (high FRET) and was unaffected by the addition of 200 nM CsdA (Fig. 4B). In contrast, at 4 mM $MgCl_2$ + NTPs, the now unstable rRNA structure was rapidly unwound by CsdA (k_{obs} = 0.70 s^{-1}, Supplementary Table S6). Nevertheless, brief transitions to the high-FRET state showed that all RNA molecules experienced cycles of folding and unfolding, although they were mostly unfolded at low Mg^{2+} (Fig. 4C). Next, we introduced two mismatch mutations (G35A, C36A) into 16S h3 that is adjacent to the donor and acceptor fluorophores. At 10 mM $MgCl_2$ + NTPs, the mutant rRNA rapidly fluctuated between high- and low-FRET states, indicating that the destabilized h3 is frequently unwound by CsdA (Fig. 4D), in agreement with our results so far. However, the h3 mutant in 10 mM $MgCl_2$ refolded more quickly than the WT rRNA in 4 mM $MgCl_2$ (compare Fig. 4C and D). This result indicated that the 16S 5′ domain remains folded overall, and that stable interactions elsewhere help h3 refold after each CsdA cycle. Altogether, these observations suggested that unwinding by CsdA depends on the local stability of the RNA interactions, but that unfolding of an entire domain depends on its global stability.

Ribosomal proteins drive reassembly and compete against CsdA unfolding

Since ribosomal proteins stabilize the native rRNA and reinforce cooperative interactions within each domain of the ribosome [61], we investigated to what extent they hamper unfolding by CsdA and rebalance the system toward native RNP assembly. We assembled fluorophore-labeled 5′ domain rRNA (Fig. 5A) with S4 alone or with ribosomal proteins S4, S16, S17, and S20 that together form a stable RNP corresponding to the body of the 30S ribosome [33, 58, 62]. When 20 nM CsdA was added to the S4–5′ domain complex, an alignment of single-molecule trajectories showed that the fluorophore-labeled rRNA fluctuated between high- and low-FRET conformations both before and after a persistent un-

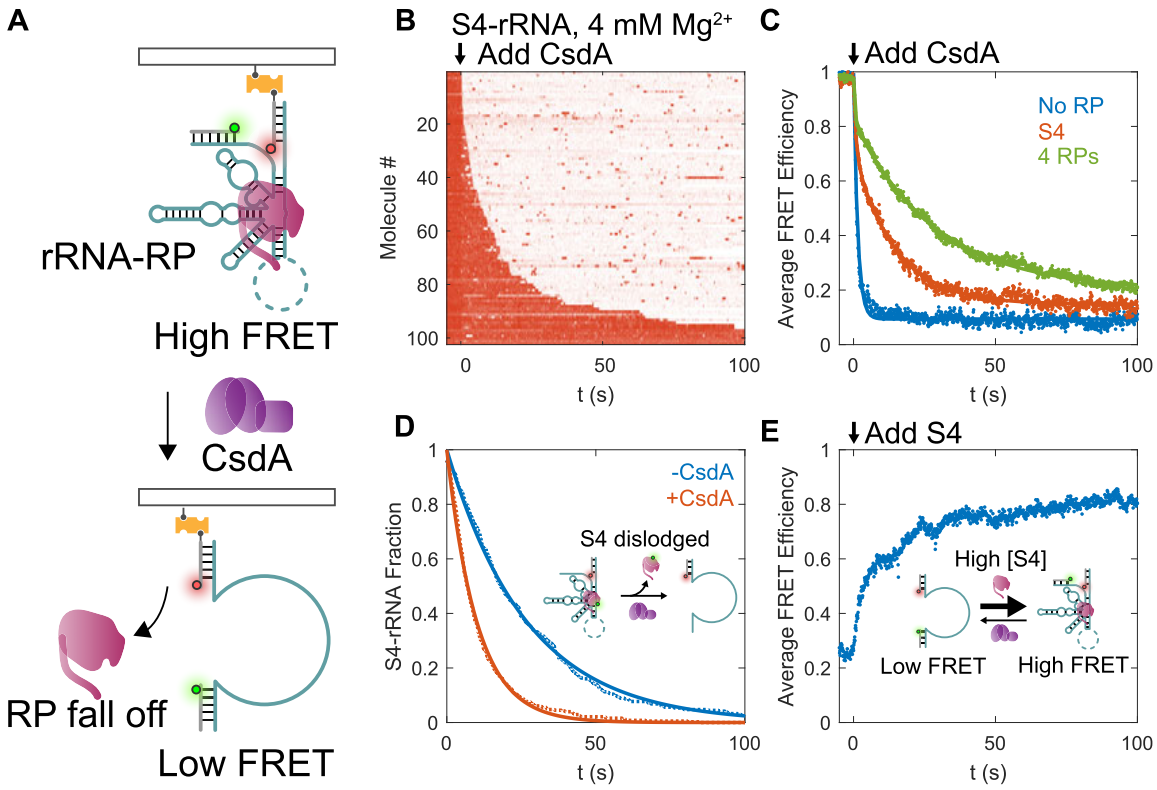

Figure 5. RNP disassembly by CsdA promotes a dynamic search for stable complexes. (**A**) smFRET assay for CsdA unfolding rRNA–protein complexes, as in Fig. 4A. In this experiment, RNA unfolding is coupled to protein dissociation. (**B**) Rastergram for rRNA–S4 complexes unfolding. See Supplementary Fig. S9 for results with no proteins and four proteins. (**C**) Ribosomal proteins (RPs) impede unfolding by CsdA. Refolded 5′ domain RNA in 4 mM $MgCl_2$ was challenged with 20 nM CsdA at time 0, as in panel (B). Symbols, the mean FRET efficiency of all molecules versus time; solid curves, fitted exponential decay. Blue, no protein; orange, RNA pre-complexed with S4; green, pre-formed S4–S16–S17–S20 RNP. See Supplementary Table S6 for fit parameters. Oscillations in the average FRET efficiency arise from statistical effects due to the number of molecules and the large change in FRET efficiency upon unfolding. (**D**) CsdA displaces S4 from the rRNA. Cy3-S4 was complexed with refolded Cy5-5′ domain rRNA, and the survival of immobilized high-FRET complexes tracked over time. Blue, −CsdA ($k = 0.037\ s^{-1}$); orange, +20 nM CsdA ($k = 0.099\ s^{-1}$). (**E**) S4 recaptures the folded RNA after it is unfolded by CsdA. Average FRET efficiency of unfolded 5′ domain RNAs in 4 mM $MgCl_2$ + 20 nM CsdA (low FRET); 10 nM S4 was added at $t = 0$; 20 nM CsdA was present throughout the movie. See Supplementary Table S3 for numbers of molecules and replicates.

folding transition (Fig. 5B and Supplementary Fig. S9A and B). The average loss of FRET efficiency over the population of molecules revealed the unfolding kinetics of each complex (Fig. 5C). The S4–5′ domain complexes were unfolded more slowly ($k_{obs} = 0.07\ s^{-1}$) than rRNA alone ($k_{obs} = 0.7\ s^{-1}$; Fig. 5C and Supplementary Table S6). The complete 5′ domain RNP was unfolded even more slowly than complexes with S4 alone ($k_{obs} = 0.035\ s^{-1}$; Fig. 5C and Supplementary Fig. S9B). This supported our expectation that disassembly by CsdA becomes less favorable as more ribosomal proteins bind the rRNA.

We next asked whether CsdA can actively dislodge ribosomal proteins. We tested this by complexing Cy5-5′ domain rRNA with Cy3-S4 protein, and then monitoring the survival of immobilized high-FRET S4–rRNA complexes over time (Fig. 5D). Any dissociated Cy3-S4 is unlikely to rebind the RNA during the movie, because its concentration is <1 pM. At 4 mM $MgCl_2$, Cy3-S4 spontaneously disassociated from the rRNA over 1 min ($k_{off} = 0.037\ s^{-1}$). In the presence of 20 nM CsdA, Cy3-S4 unbinding was ~3-fold faster ($k_{off} = 0.099\ s^{-1}$). Thus, CsdA not only unfolds the rRNA but also accelerates the disassembly of unstable RNPs.

For ribosome assembly to proceed, ribosomal proteins must capture the transiently refolded rRNA in the presence of chaperones. We demonstrated this idea by adding 10 nM S4 to Cy3–Cy5-labeled 5′ domain rRNA that had already been unfolded by CsdA (Fig. 5E). Although CsdA was still present, the addition of S4 increased the fraction of folded rRNA, as reflected by an increase in the average FRET efficiency from 0.2 (mostly unfolded) to 0.8 (mostly folded) over 40 s (Fig. 5E). Trajectories of single molecules showed that individual RNAs continued to sample the low-FRET state after refolding (Supplementary Fig. S9C), indicating that CsdA remained active throughout the video. However, most RNA molecules continued to favor the high-FRET state once refolded, suggesting that local unwinding by CsdA cannot dissociate the complex after S4 is stably bound. This result showed that S4, when present in excess, is able to capture its binding site and protect the rRNA from unfolding by CsdA. This result also helped explain why multiprotein RNPs resist CsdA disassembly more than single-protein RNPs.

30S ribosomes are protected from CsdA unwinding

Because CsdA preferentially disassembles unstable ribosomal complexes, we tested whether native 30S ribosomal subunits or reconstituted 30S complexes can avoid unfolding by CsdA. We used oligonucleotide-directed RNase H cleavage [63, 64] to determine whether CsdA can disrupt 30S complexes and expose the 16S rRNA to hybridization with antisense DNA

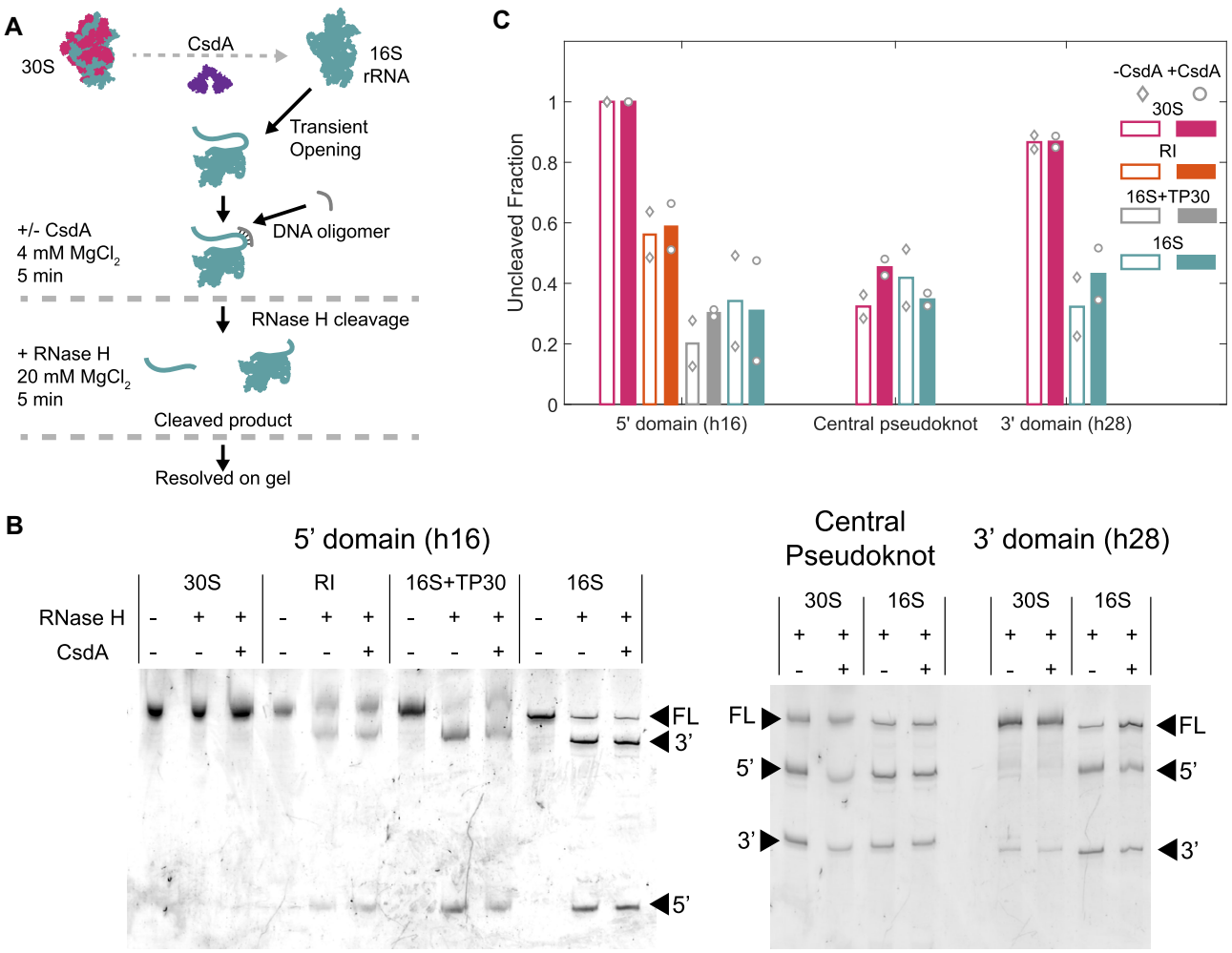

Figure 6. CsdA does not disassemble native 30S ribosomes at low magnesium. (**A**) RNase H assay for 30S disassembly and exposure of the 16S rRNA. 30S complexes were allowed to hybridize with antisense DNA in the presence of 200 nM CsdA and 4 mM $MgCl_2$ (low stability). Complexes were restabilized in 20 mM $MgCl_2$ before treatment with RNase H. (**B**) Cleavage products (6% PAGE with SYBR Gold stain). Antisense oligomers targeted the indicated 16S helices. 30S, native 30S ribosomes; 16S, native 16S rRNA; RI, reconstitution intermediate of 16S and TP30 at 30°C; 16S + TP30, 16S was mixed with TP30 and immediately treated with CsdA. Bands corresponding to full-length 16S, and 5′ and 3′ products are indicated. (**C**) Fraction of full-length rRNA (uncleaved) after RNase H treatment. Symbols, individual replicates; bars, mean value. Open bars and diamonds, no CsdA; filled bars and circles, +CsdA. On average, CsdA fails to disassemble 30S ribosomes or persistently unfold stable 16S helices under these conditions.

oligonucleotides (AONs) (Fig. 6A). AONs complementary to h16 in the 16S 5′ domain, the central pseudoknot, and h28 in the 16S 3′ domain were added to complexes at 4 mM $MgCl_2$ together with CsdA. After a period of unwinding, the complexes were restabilized with 20 mM $MgCl_2$. The trapped DNA–RNA hybrids were cleaved by RNase H and the products resolved by PAGE (Fig. 6B).

In the presence of anti-h16 or anti-h28 AONs, native 30S subunits were protected from RNase H cleavage compared to the 16S rRNA alone (Fig. 6C). 16S rRNA reconstituted with 30S proteins (TP30) was partially protected, whereas rRNA mixed with TP30 was not protected (Fig. 6C). Importantly, CsdA did not increase the fraction of cleaved rRNA, indicating that CsdA was not able to persistently disrupt native 30S ribosomes and convert them to the equivalent of free 16S rRNA. The 30S central pseudoknot was cleaved under all conditions, presumably because it is unstable at low magnesium concentration [65, 66].

To test whether CsdA unfolds 30S ribosomes *in vivo*, we transformed a WT strain (BW25113) and a strain lacking the assembly factor RbfA (Δ*rbfA*) with plasmids that overexpress CsdA or CsdA-DQAD from an IPTG-inducible promoter. The assembly factor RbfA binds 30S and pre-30S ribosomes and stabilizes the active site during late steps of 30S biogenesis [67, 68] and quality control [69]. Deletion of RbfA leads to an accumulation of pre-30S complexes at low temperatures [67, 68], potentially sensitizing the strain to RNA chaperones. Consistent with previous studies [28, 70], CsdA overexpression resulted in fewer colonies at 37°C (Fig. 7) and at 30°C (Supplementary Fig. S10), for both WT and Δ*rbfA* strains. This dominant negative effect depended only partly on the ATPase activity of CsdA, since CsdA-DQAD overexpression was also toxic, albeit to a lesser extent. Because CsdA overexpression did not rescue the *rbfA* deletion, we concluded that additional CsdA activity cannot compensate for the lack of specific 30S assembly factors.

Discussion

rRNA is often assumed to fold natively during transcription, explaining the tight coupling between transcription elongation and assembly first observed in electron micrographs of

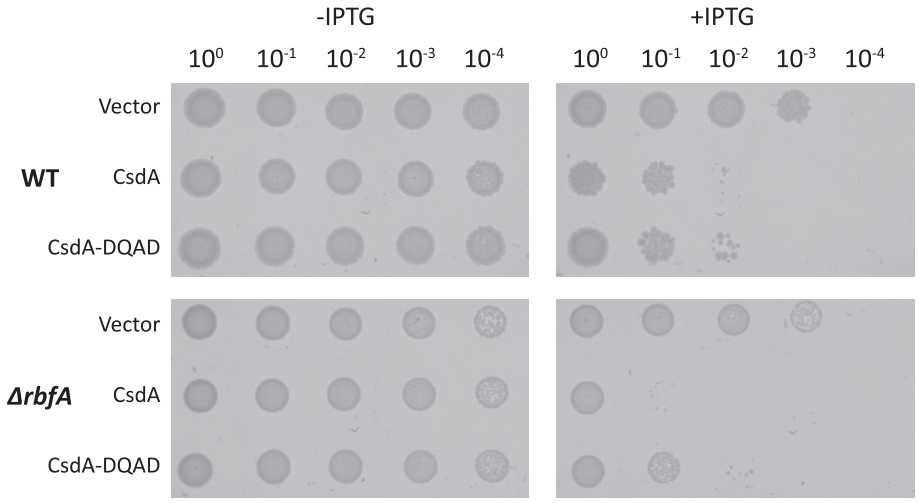

Figure 7. CsdA or CsdA-DQAD overexpression does not compensate deletion of RbfA. *Escherichia coli* strains BW25113 (WT) or BW25113Δ*rbfA* were transformed with plasmids expressing WT CsdA (pMAL-p5X-CsdA), inactive CsdA-DQAD (pMAL-p5X-CsdA-DQAD), or vector (pMAL-p5X). Serial dilutions of the indicated strains were spotted on LB agar with or without IPTG, and incubated at 37°C for 24 h ($n = 3$). See Supplementary Fig. S10 for data at 30°C.

active chromatin [1]. In contrast, single-molecule cotranscriptional assembly experiments showed that the pre-rRNA often misfolds during transcription *in vitro* [5, 6], raising the question of how efficient ribosome biogenesis is obtained in cells.

In this study, we show that the ATP-dependent DEAD-box chaperone CsdA (DeaD) greatly accelerates recruitment of ribosomal protein S4 to the nascent rRNA, which is one of the first steps of bacterial 30S assembly. CsdA promotes stable S4 binding to its correct site in the 16S rRNA and reduces the frequency of transient binding to nonspecific sites (Figs 1 and 2). The improvement in S4 recruitment is equivalent to that achieved by thermal renaturation of the rRNA, indicating that CsdA acts by resolving rRNA conformations that are incompetent for S4 binding (Fig. 3). Overall, these results suggest that DEAD-box proteins and other RNA chaperones may participate in transcription-coupled assembly more widely than previously realized, overcoming the tendency of nascent transcripts to be kinetically trapped in local structures [71]. In this sense, cotranscriptional folding of RNA may be akin to the chaperoned folding of nascent polypeptide chains.

Our experiments do not reveal to what degree the nascent rRNA is misfolded. Mispairing of even a few nucleotides at helix junctions, however, would disrupt the rRNA tertiary structure and forbid S4 binding [51, 54, 64, 72]. Even small defects may require an RNA helicase to resolve if they are coupled to protein binding or RNA tertiary interactions [17, 73].

Previous studies found that the DEAD-box proteins CYT-19 and Mss116p refold ribozymes through iterative annealing [10–12]. In the classic iterative annealing model, RNA unwinding coupled to ATP hydrolysis pumps the RNA out of metastable states, providing another chance for it to fold (Fig. 8). We show that CsdA not only unwinds rRNA, but dissociates unstable S4 complexes. Free S4 protein recaptures the refolded rRNA, protecting it from further unfolding. Thus, CsdA unwinding stimulates cycles of assembly and disassembly that fuel the search for the native RNP.

DEAD-box proteins are widespread in nature, participating in ribosome biogenesis and many other steps of RNA metabolism [24, 74, 75]. Many DEAD-box proteins are recruited to ribosome assembly intermediates through RNA or protein interactions, and act on specific targets [17, 76, 77]. For example, the *E. coli* DEAD-box protein DbpA is activated by a specific sequence in the 23S rRNA [78, 79]. In contrast, CsdA appears to function as a general RNA chaperone, whose activity depends only on the stability of the RNA helices it encounters.

Because ribosome assembly intermediates gain stability as more proteins add to the complex, the rRNA should become less susceptible to chaperone unwinding as assembly progresses (Fig. 8). In agreement with this expectation, we found that CsdA unfolded 5′ domain RNPs more slowly than S4 complexes (Fig. 5), and was unable to disassemble 30S ribosomes *in vitro* (Fig. 6). Our single-molecule trajectories showed that RNAs experience multiple short-lived unwinding events before complete unfolding (Figs 4 and 5). Stable complexes may quickly relax to the native structure after local unwinding by CsdA, preserving the integrity of the complex. In contrast, unstable or misassembled complexes may be less able to recover from local unwinding, and unfold.

From these observations, we propose that general ATP-dependent chaperones such as CsdA create a disassembly gradient in cells that opposes normal ribosome assembly, depleting misassembled intermediates while allowing native-like intermediates to continue (Fig. 8). We previously found that cotranscriptional assembly becomes more efficient when multiple ribosomal proteins can interact with a transcript [6]. By pruning unstable intermediates, chaperone-driven disassembly is expected to further intensify the cooperative hierarchy of assembly.

This model implies a delicate balance in cells between chaperone activity and proteins that stabilize the rRNA structure, as also suggested by theoretical simulations of chaperone cycles [21]. Overexpression of CsdA is toxic to *E. coli*, presumably because normal RNA structures are disrupted. The inability of CsdA to compensate for deletion of the late assembly factor RbfA suggests that general chaperones are most important during the earliest cotranscriptional stages of bacterial ribosome synthesis. It will be interesting to learn how general chaperones interact with factors that facilitate specific conformational rearrangements and stabilize pre-ribosomes.

The limitation of this study is that the chaperone's activity depends on the experimental condition, such as Mg^{2+} ion

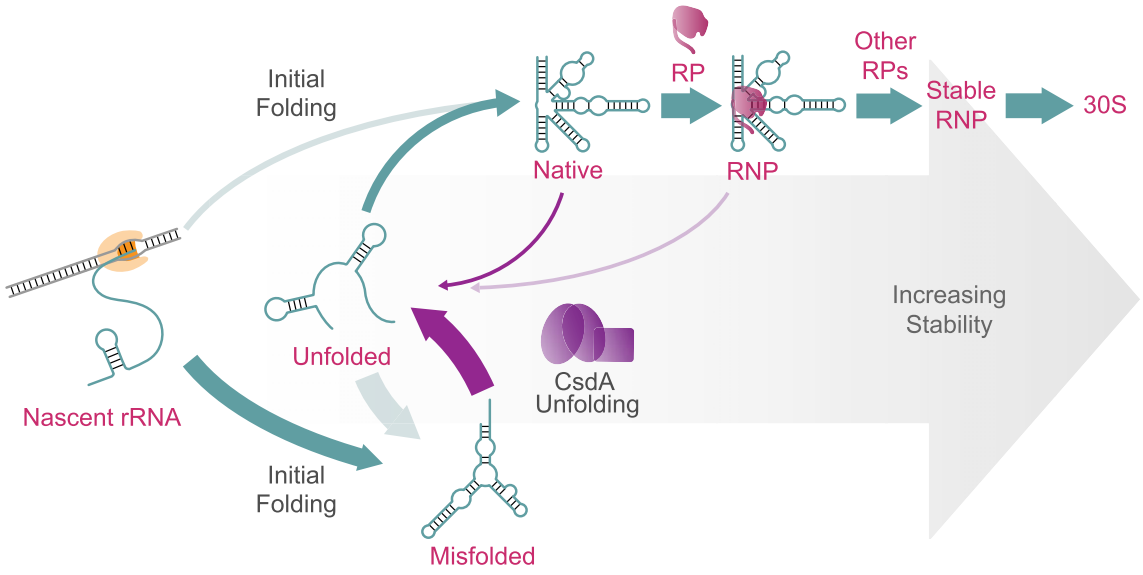

Figure 8. General chaperones facilitate ribosome assembly by acting against the gradient of RNP stability. CsdA refolds rRNA through the generalized iterative annealing mechanism. Most rRNA misfolds during transcription (dark green forward arrow), whereas only a small fraction folds natively (light green forward arrow). Spontaneous interconversion between these conformations (≥100 s) is slower than the timescale for transcription of an rRNA domain (<10 s). CsdA is expected to unfold misfolded rRNA faster than native rRNA because the native rRNA is more stable (purple reverse arrows). As assembly progresses, native intermediates become progressively worse chaperone substrates, ultimately forming mature 30S ribosomes. Disassembly of unfit RNPs by general chaperones supports the hierarchy of ribosome assembly by powering the search for low free energy structures.

concentration and chaperone concentration. Our experiments lack features of the cellular environment, which is crowded and contains all of the ribosomal proteins and assembly factors that also affect folding of the nascent rRNA. Thus, the effect of CsdA *in vitro* may not precisely correspond to its effect in cells. However, the copy number of CsdA relative to free S4 in *E. coli*. is comparable to that in our experiments [81, 82]. Thus, our system serves as a model that demonstrates the function of general DEAD-box chaperones in ribosome biogenesis.

Acknowledgements

We thank Dr Margaret Rodgers and members of the Woodson lab for helpful discussion. We acknowledge Dr Yunyu Shi for providing plasmids and Dr Margaret Rodgers, Dr Sanjaya Abeysirigunawardena, and Dr Arthur Korman for purified proteins.

Author contributions: Y.S. designed and performed experiments, analyzed data, interpreted results, and wrote the manuscript; S.A.W. interpreted results, wrote the manuscript, and obtained funding.

Supplementary data

Supplementary data is available at NAR online.

Conflict of interest

None declared.

Funding

This project was supported by a grant from the National Institute of General Medical Sciences (R35GM136351 to S.A.W.).

Funding to pay the Open Access publication charges for this article was provided by an Editorial Board Waiver.

Data availability

Data associated with this paper are available from Johns Hopkins Research Data Repository at https://doi.org/10.7281/T1/Z73MRN.

References

1. French SL, Miller OL. Transcription mapping of the *Escherichia coli* chromosome by electron microscopy. *J Bacteriol* 1989;**171**:4207–16. https://doi.org/10.1128/jb.171.8.4207-4216.1989
2. Davis JH, Williamson JR. Structure and dynamics of bacterial ribosome biogenesis. *Philos Trans R Soc B* 2017;**372**:20160181. https://doi.org/10.1098/rstb.2016.0181
3. Nomura M, Mizushima S, Ozaki M *et al.* Structure and function of ribosomes and their molecular components. *Cold Spring Harbor Symp Quant Biol* 1969;**34**:49–61. https://doi.org/10.1101/SQB.1969.034.01.009
4. Held WA, Ballou B, Mizushima S *et al.* Assembly mapping of 30S ribosomal proteins from *Escherichia coli*: further studies. *J Biol Chem* 1974;**249**:3103–11. https://doi.org/10.1016/S0021-9258(19)42644-6
5. Duss O, Stepanyuk GA, Puglisi JD *et al.* Transient protein–RNA interactions guide nascent ribosomal RNA folding. *Cell* 2019;**179**:1357–69. https://doi.org/10.1016/j.cell.2019.10.035
6. Rodgers ML, Woodson SA. Transcription increases the cooperativity of ribonucleoprotein assembly. *Cell* 2019;**179**:1370–81. https://doi.org/10.1016/j.cell.2019.11.007
7. Thirumalai D, Woodson SA. Kinetics of folding of proteins and RNA. *Acc Chem Res* 1996;**29**:433–9. https://doi.org/10.1021/ar9500933
8. Herschlag D. RNA chaperones and the RNA folding problem. *J Biol Chem* 1995;**270**:20871–4. https://doi.org/10.1074/jbc.270.36.20871

9. Woodson SA. Taming free energy landscapes with RNA chaperones. *RNA Biol* 2010;**7**:677–86. https://doi.org/10.4161/rna.7.6.13615
10. Mohr S, Stryker JM, Lambowitz AM. A DEAD-box protein functions as an ATP-dependent RNA chaperone in group I intron splicing. *Cell* 2002;**109**:769–79. https://doi.org/10.1016/S0092-8674(02)00771-7
11. Bhaskaran H, Russell R. Kinetic redistribution of native and misfolded RNAs by a DEAD-box chaperone. *Nature* 2007;**449**:1014–8. https://doi.org/10.1038/nature06235
12. Del Campo M, Tijerina P, Bhaskaran H *et al.* Do DEAD-box proteins promote group II intron splicing without unwinding RNA? *Mol Cell* 2007;**28**:159–66. https://doi.org/10.1016/j.molcel.2007.07.028
13. Fedorova O, Solem A, Pyle AM. Protein-facilitated folding of group II intron ribozymes. *J Mol Biol* 2010;**397**:799–813. https://doi.org/10.1016/j.jmb.2010.02.001
14. Karunatilaka KS, Solem A, Pyle AM *et al.* Single-molecule analysis of Mss116-mediated group II intron folding. *Nature* 2010;**467**:935–9. https://doi.org/10.1038/nature09422
15. Hilbert M, Karow AR, Klostermeier D. The mechanism of ATP-dependent RNA unwinding by DEAD box proteins. *Biol Chem* 2009;**390**:1237–50.
16. Yang Q, Del Campo M, Lambowitz AM *et al.* DEAD-box proteins unwind duplexes by local strand separation. *Mol Cell* 2007;**28**:253–63. https://doi.org/10.1016/j.molcel.2007.08.016
17. Cruz VE, Sekulski K, Peddada N *et al.* Sequence-specific remodeling of a topologically complex RNP substrate by Spb4. *Nat Struct Mol Biol* 2022;**29**:1228–38. https://doi.org/10.1038/s41594-022-00874-9
18. Jankowsky E. RNA helicases at work: binding and rearranging. *Trends Biochem Sci* 2011;**36**:19–29. https://doi.org/10.1016/j.tibs.2010.07.008
19. Todd MJ, Lorimer GH, Thirumalai D. Chaperonin-facilitated protein folding: optimization of rate and yield by an iterative annealing mechanism. *Proc Natl Acad Sci USA* 1996;**93**:4030–5. https://doi.org/10.1073/pnas.93.9.4030
20. Chakrabarti S, Hyeon C, Ye X *et al.* Molecular chaperones maximize the native state yield on biological times by driving substrates out of equilibrium. *Proc Natl Acad Sci USA* 2017;**114**:E10919–27. https://doi.org/10.1073/pnas.1712962114
21. Song Y, Thirumalai D, Hyeon C. Moderate activity of RNA chaperone maximizes the yield of self-spliced pre-RNA *in vivo*. *Proc Natl Acad Sci USA* 2022;**119**:e2209422119. https://doi.org/10.1073/pnas.2209422119
22. de la Cruz J, Kressler D, Linder P. Unwinding RNA in *Saccharomyces cerevisiae*: DEAD-box proteins and related families. *Trends Biochem Sci* 1999;**24**:192–8. https://doi.org/10.1016/S0968-0004(99)01376-6
23. Mitterer V, Pertschy B. RNA folding and functions of RNA helicases in ribosome biogenesis. *RNA Biol* 2022;**19**:781–810. https://doi.org/10.1080/15476286.2022.2079890
24. Bohnsack KE, Yi S, Venus S *et al.* Cellular functions of eukaryotic RNA helicases and their links to human diseases. *Nat Rev Mol Cell Biol* 2023;**24**:749–69. https://doi.org/10.1038/s41580-023-00628-5
25. Redder P, Hausmann S, Khemici V *et al.* Bacterial versatility requires DEAD-box RNA helicases. *FEMS Microbiol Rev* 2015;**39**:392–412. https://doi.org/10.1093/femsre/fuv011
26. Jones PG, Mitta M, Kim Y *et al.* Cold shock induces a major ribosomal-associated protein that unwinds double-stranded RNA in *Escherichia coli*. *Proc Natl Acad Sci USA* 1996;**93**:76–80. https://doi.org/10.1073/pnas.93.1.76
27. Vakulskas CA, Pannuri A, Cortés-Selva D *et al.* Global effects of the DEAD-box RNA helicase DeaD (CsdA) on gene expression over a broad range of temperatures. *Mol Microbiol* 2014;**92**:945–58. https://doi.org/10.1111/mmi.12606
28. Charollais J, Dreyfus M, Iost I. CsdA, a cold-shock RNA helicase from *Escherichia coli*, is involved in the biogenesis of 50S ribosomal subunit. *Nucleic Acids Res* 2004;**32**:2751–9. https://doi.org/10.1093/nar/gkh603
29. Jagessar KL, Jain C. Functional and molecular analysis of *Escherichia coli* strains lacking multiple DEAD-box helicases. *RNA* 2010;**16**:1386–92. https://doi.org/10.1261/rna.2015610
30. Moll I, Grill S, Gründling A *et al.* Effects of ribosomal proteins S1, S2 and the DeaD/CsdA DEAD-box helicase on translation of leaderless and canonical mRNAs in *Escherichia coli*. *Mol Microbiol* 2002;**44**:1387–96. https://doi.org/10.1046/j.1365-2958.2002.02971.x
31. Reisch CR, Prather KLJ. The no-SCAR (Scarless Cas9 Assisted Recombineering) system for genome editing in *Escherichia coli*. *Sci Rep* 2015;**5**:15096. https://doi.org/10.1038/srep15096
32. Reisch CR, Prather KLJ. Scarless Cas9 assisted recombineering (no-SCAR) in *Escherichia coli*, an easy-to-use system for genome editing. *Curr Protoc Mol Biol* 2017;**117**:31.8.1–20. https://doi.org/10.1002/cpmb.29
33. Abeysirigunawardena SC, Kim H, Lai J *et al.* Evolution of protein-coupled RNA dynamics during hierarchical assembly of ribosomal complexes. *Nat Commun* 2017;**8**:492. https://doi.org/10.1038/s41467-017-00536-1
34. Davanloo P, Rosenberg AH, Dunn JJ *et al.* Cloning and expression of the gene for bacteriophage T7 RNA polymerase. *Proc Natl Acad Sci USA* 1984;**81**:2035–9. https://doi.org/10.1073/pnas.81.7.2035
35. Culver GM, Noller HF. Efficient reconstitution of functional *Escherichia coli* 30S ribosomal subunits from a complete set of recombinant small subunit ribosomal proteins. *RNA* 1999;**5**:832–43. https://doi.org/10.1017/S1355838299990714
36. Xu L, Wang L, Peng J *et al.* Insights into the structure of dimeric RNA helicase CsdA and indispensable role of its C-terminal regions. *Structure* 2017;**25**:1795–808. https://doi.org/10.1016/j.str.2017.09.013
37. Bellur DL, Woodson SA. A minimized rRNA-binding site for ribosomal protein S4 and its implications for 30S assembly. *Nucleic Acids Res* 2009;**37**:1886–96. https://doi.org/10.1093/nar/gkp036
38. Kim H, Abeysirigunawarden SC, Chen K *et al.* Protein-guided RNA dynamics during early ribosome assembly. *Nature* 2014;**506**:334–8. https://doi.org/10.1038/nature13039
39. Roy R, Hohng S, Ha T. A practical guide to single-molecule FRET. *Nat Methods* 2008;**5**:507–16. https://doi.org/10.1038/nmeth.1208
40. Hua B, Han KY, Zhou R *et al.* An improved surface passivation method for single-molecule studies. *Nat Methods* 2014;**11**:1233–6. https://doi.org/10.1038/nmeth.3143
41. Spedding G. *Ribosomes and Protein Synthesis: A Practical Approach*. Oxford, UK: Oxford University Press, 1990.
42. Friedman LJ, Gelles J. Multi-wavelength single-molecule fluorescence analysis of transcription mechanisms. *Methods* 2015;**86**:27–36. https://doi.org/10.1016/j.ymeth.2015.05.026
43. Kaur H, Jamalidinan F, Condon SGF *et al.* Analysis of spliceosome dynamics by maximum likelihood fitting of dwell time distributions. *Methods* 2019;**153**:13–21. https://doi.org/10.1016/j.ymeth.2018.11.014
44. Nowotny V, Nierhaus KH. Assembly of the 30S subunit from *Escherichia coli* ribosomes occurs via two assembly domains which are initiated by S4 and S7. *Biochemistry* 1988;**27**:7051–5. https://doi.org/10.1021/bi00418a057
45. Stern S, Wilson RC, Noller HF. Localization of the binding site for protein S4 on 16S ribosomal RNA by chemical and enzymatic probing and primer extension. *J Mol Biol* 1986;**192**:101–10. https://doi.org/10.1016/0022-2836(86)90467-5
46. Vartikar JV, Draper DE. S4–16S ribosomal RNA complex: binding constant measurements and specific recognition of a 460-nucleotide region. *J Mol Biol* 1989;**209**:221–34. https://doi.org/10.1016/0022-2836(89)90274-X
47. Gerstner RB, Pak Y, Draper DE. Recognition of 16S rRNA by ribosomal protein S4 from *Bacillus stearothermophilus*.

Biochemistry 2001;**40**:7165–73. https://doi.org/10.1021/bi010026i
48. Mayerle M, Woodson SA. Specific contacts between protein S4 and ribosomal RNA are required at multiple stages of ribosome assembly. *RNA* 2013;**19**:574–85. https://doi.org/10.1261/rna.037028.112
49. Powers T, Noller HF. A temperature-dependent conformational rearrangement in the ribosomal protein S4·16S rRNA complex. *J Biol Chem* 1995;**270**:1238–42. https://doi.org/10.1074/jbc.270.3.1238
50. Adilakshmi T, Bellur DL, Woodson SA. Concurrent nucleation of 16S folding and induced fit in 30S ribosome assembly. *Nature* 2008;**455**:1268–72. https://doi.org/10.1038/nature07298
51. Mayerle M, Bellur DL, Woodson SA. Slow formation of stable complexes during coincubation of minimal rRNA and ribosomal protein S4. *J Mol Biol* 2011;**412**:453–65. https://doi.org/10.1016/j.jmb.2011.07.048
52. Chen K, Eargle J, Lai J *et al.* Assembly of the five-way junction in the ribosomal small subunit using hybrid MD-Gō simulations. *J Phys Chem B* 2012;**116**:6819–31. https://doi.org/10.1021/jp212614b
53. Hwang H, Kim H, Myong S. Protein induced fluorescence enhancement as a single molecule assay with short distance sensitivity. *Proc Natl Acad Sci USA* 2011;**108**:7414–8. https://doi.org/10.1073/pnas.1017672108
54. Adilakshmi T, Ramaswamy P, Woodson SA. Protein-independent folding pathway of the 16S rRNA 5′ domain. *J Mol Biol* 2005;**351**:508–19. https://doi.org/10.1016/j.jmb.2005.06.020
55. Bizebard T, Ferlenghi I, Iost I *et al.* Studies on three *E. coli* DEAD-box helicases point to an unwinding mechanism different from that of model DNA helicases. *Biochemistry* 2004;**43**:7857–66. https://doi.org/10.1021/bi049852s
56. Halls C, Mohr S, Del Campo M *et al.* Involvement of DEAD-box proteins in group I and group II intron splicing. Biochemical characterization of Mss116p, ATP hydrolysis-dependent and -independent mechanisms, and general RNA chaperone activity. *J Mol Biol* 2007;**365**:835–55. https://doi.org/10.1016/j.jmb.2006.09.083
57. Thirumalai D, Lorimer GH, Hyeon C. Iterative annealing mechanism explains the functions of the GroEL and RNA chaperones. *Protein Sci* 2020;**29**:360–77. https://doi.org/10.1002/pro.3795
58. Ramaswamy P, Woodson SA. S16 throws a conformational switch during assembly of 30S 5′ domain. *Nat Struct Mol Biol* 2009;**16**:438–45. https://doi.org/10.1038/nsmb.1585
59. Yang Q, Fairman ME, Jankowsky E. DEAD-box-protein-assisted RNA structure conversion towards and against thermodynamic equilibrium values. *J Mol Biol* 2007;**368**:1087–100. https://doi.org/10.1016/j.jmb.2007.02.071
60. Stampfl S, Doetsch M, Beich-Frandsen M *et al.* Characterization of the kinetics of RNA annealing and strand displacement activities of the *E. coli* DEAD-box helicase CsdA. *RNA Biol* 2013;**10**:149–56. https://doi.org/10.4161/rna.23475
61. Ramaswamy P, Woodson SA. Global stabilization of rRNA structure by ribosomal proteins S4, S17 and S20. *J Mol Biol* 2009;**392**:666–77. https://doi.org/10.1016/j.jmb.2009.07.032
62. Weitzmann CJ, Cunningham PR, Nurse K *et al.* Chemical evidence for domain assembly of the *Escherichia coli* 30S ribosome. *FASEB J* 1993;**7**:177–80. https://doi.org/10.1096/fasebj.7.1.7916699
63. Treiber DK, Williamson JR. Kinetic oligonucleotide hybridization for monitoring kinetic folding of large RNAs. *Methods Enzymol* 2000;**317**:330–53.
64. Sharma IM, Rappé MC, Addepalli B *et al.* A metastable rRNA junction essential for bacterial 30S biogenesis. *Nucleic Acids Res* 2018;**46**:5182–94. https://doi.org/10.1093/nar/gky120
65. Holmes KL, Culver GM. Mapping structural differences between 30S ribosomal subunit assembly intermediates. *Nat Struct Mol Biol* 2004;**11**:179–86. https://doi.org/10.1038/nsmb719
66. Clatterbuck Soper SF, Dator RP, Limbach PA *et al. In vivo* X-ray footprinting of pre-30S ribosomes reveals chaperone-dependent remodeling of late assembly intermediates. *Mol Cell* 2013;**52**:506–16. https://doi.org/10.1016/j.molcel.2013.09.020
67. Jones PG, Inouye M. RbfA, a 30S ribosomal binding factor, is a cold-shock protein whose absence triggers the cold-shock response. *Mol Microbiol* 1996;**21**:1207–18. https://doi.org/10.1111/j.1365-2958.1996.tb02582.x
68. Xia B, Ke H, Shinde U *et al.* The role of RbfA in 16S rRNA processing and cell growth at low temperature in *Escherichia coli*. *J Mol Biol* 2003;**332**:575–84. https://doi.org/10.1016/S0022-2836(03)00953-7
69. Sharma IM, Woodson SA. RbfA and IF3 couple ribosome biogenesis and translation initiation to increase stress tolerance. *Nucleic Acids Res* 2020;**48**:359–72.
70. Sheng K, Li N, Rabuck-Gibbons JN *et al.* Assembly landscape for the bacterial large ribosomal subunit. *Nat Commun* 2023;**14**:5220. https://doi.org/10.1038/s41467-023-40859-w
71. Rodgers ML, Woodson SA. A roadmap for rRNA folding and assembly during transcription. *Trends Biochem Sci* 2021;**46**:889–901. https://doi.org/10.1016/j.tibs.2021.05.009
72. Huang H, Karbstein K. Assembly factors chaperone ribosomal RNA folding by isolating helical junctions that are prone to misfolding. *Proc Natl Acad Sci USA* 2021;**118**:e2101164118. https://doi.org/10.1073/pnas.2101164118
73. Cruz VE, Weirich CS, Peddada N *et al.* The DEAD-box ATPase Dbp10/DDX54 initiates peptidyl transferase center formation during 60S ribosome biogenesis. *Nat Commun* 2024;**15**:3296. https://doi.org/10.1038/s41467-024-47616-7
74. Linder P, Jankowsky E. From unwinding to clamping—the DEAD box RNA helicase family. *Nat Rev Mol Cell Biol* 2011;**12**:505–16. https://doi.org/10.1038/nrm3154
75. Pyle AM. RNA helicases and remodeling proteins. *Curr Opin Chem Biol* 2011;**15**:636–42. https://doi.org/10.1016/j.cbpa.2011.07.019
76. Dembowski JA, Kuo B, Woolford JL Jr. Has1 regulates consecutive maturation and processing steps for assembly of 60S ribosomal subunits. *Nucleic Acids Res* 2013;**41**:7889–904. https://doi.org/10.1093/nar/gkt545
77. Khreiss A, Capeyrou R, Lebaron S *et al.* The DEAD-box protein Dbp6 is an ATPase and RNA annealase interacting with the peptidyl transferase center (PTC) of the ribosome. *Nucleic Acids Res* 2023;**51**:744–64. https://doi.org/10.1093/nar/gkac1196
78. Wurm JP, Glowacz K-A, Sprangers R. Structural basis for the activation of the DEAD-box RNA helicase DbpA by the nascent ribosome. *Proc Natl Acad Sci USA* 2021;**118**:e2105961118. https://doi.org/10.1073/pnas.2105961118
79. Fuller-Pace FV, Nicol SM, Reid AD *et al.* DbpA: a DEAD box protein specifically activated by 23S rRNA. *EMBO J* 1993;**12**:3619–26. https://doi.org/10.1002/j.1460-2075.1993.tb06035.x
80. Dunkle JA, Wang L, Feldman MB *et al.* Structures of the bacterial ribosome in classical and hybrid states of tRNA binding. *Science* 2011;**332**:981–4. https://doi.org/10.1126/science.1202692
81. Li GW, Burkhardt D, Gross C *et al.* Quantifying absolute protein synthesis rates reveals principles underlying allocation of cellular resources. *Cell* 2014;**157**:624–35. https://doi.org/10.1016/j.cell.2014.02.033
82. Chen SS, Sperling E, Silverman JM *et al.* Measuring the dynamics of E. coli ribosome biogenesis using pulse-labeling and quantitative mass spectrometry. *Mol Biosyst* 2012;**8**:3325–34. https://doi.org/10.1039/c2mb25310k

Received: October 10, 2024. **Revised:** January 27, 2025. **Editorial Decision:** January 29, 2025. **Accepted:** February 5, 2025